

GYROSYNCHROTRON EMISSION FROM ANISOTROPIC ELECTRON DISTRIBUTIONS

G. D. FLEISHMAN^{1,2,3} AND V. F. MELNIKOV⁴

Received 2002 July 30; accepted 2002 December 22

ABSTRACT

We present numerical calculations of the intensity, degree of polarization, and spectral index of gyro-synchrotron emission produced by fast electrons with anisotropic pitch-angle distributions. The anisotropy is found to affect the emission substantially. The emission intensity can change up to a few orders of magnitude at the optically thin region compared with the isotropic case. The local value of spectral index changes considerably with the anisotropy. *X*-mode polarization increases for loss cone distributions and decreases for beamlike distributions. Moreover, the sense of polarization can correspond to the ordinary wave mode at the optically thin region for a certain range of view angles for beamlike distributions. We discuss possible applications and observability of the effects obtained.

Subject headings: acceleration of particles — radiation mechanisms: nonthermal — Sun: flares

1. INTRODUCTION

Soon after synchrotron radiation had been proposed as a mechanism for cosmic nonthermal radio emission (Alfvén & Herlofson 1950; Kiepenheuer 1950), it was found (Korchak & Terletsky 1952; Getmantsev 1952; Korchak 1957; Syrovatsky 1959) that a power-law distribution of ultrarelativistic charged particles produced the emission with a power-law spectrum in the optically thin range. After that, the detailed theory of the cosmic synchrotron spectrum (Twiss 1954; Trubnikov 1958; Razin 1960a) and polarization (Garibyan & Goldman 1954; Sokolov & Ternov 1956; Westfold 1959) was developed. While the ultrarelativistic approximation is sufficient for most of the cosmic objects (Ginzburg & Syrovatsky 1964), it is not correct for the solar case (Ramaty 1969; Takakura 1972; Ramaty & Petrosian 1972).

Thus, a lot of effort has been made to find simple approximations that are valid for gyrosynchrotron emission produced by nonrelativistic and moderately relativistic electrons (Petrosian 1981; Grebinskii & Sedov 1982; Dulk & Marsh 1982; Robinson 1985; Klein 1987; Zhou et al. 1998; Zhou, Huang, & Wang 1999) or to perform exact numerical calculations (Hildebrandt & Krüger 1996; Belkora 1997).

While the general formalism (Ramaty 1969) allows for arbitrary pitch-angle anisotropy, most of the papers focused on isotropic distributions of fast electrons. A few exceptions only consider weakly anisotropic pitch-angle distributions (Petrosian 1981; Robinson 1985; Klein 1987). The authors of the papers did not find any significant effect of the pitch-angle anisotropy on the spectrum and polarization of the optically thin part of the gyrosynchrotron emission.

Synchrotron radiation by a single ultrarelativistic electron is characterized by prominent directivity along the

particle velocity. Indeed, most of the energy is emitted within a narrow cone,

$$\vartheta \sim \gamma_e^{-1} = mc^2/E, \quad (1)$$

along the velocity, where γ_e is the Lorentz factor of the electron, m and E are the mass and energy of the electron, and c is the speed of light; so $\vartheta \ll 1$, if $\gamma_e \gg 1$. Only extremely strong anisotropy (when the electron distribution function changes noticeably within the small angle; eq. [1]) can affect synchrotron emission produced by an ensemble of ultrarelativistic electrons. Hence, any expected anisotropy is entirely unimportant to calculate synchrotron emission from distant objects such as supernova remnants or radio galaxies.

However, this does not hold for the solar case in which semirelativistic and mildly relativistic electrons contribute the bulk of the gyrosynchrotron emission. Thus, the anisotropy (if present) is potentially important for the modeling of solar microwave continuum bursts (commonly believed to be produced by gyrosynchrotron mechanism; Bastian et al. 1998).

Actually, there is presently ample evidence of the anisotropic pitch-angle distributions of energetic electrons in solar flares. Analysis of particle kinetics effects on the temporal and spectral behavior of optically thin microwave and hard X-ray emissions (Melnikov 1994; Melnikov & Magun 1998; Melnikov & Silva 2000; Lee & Gary 2000) indicates that a considerable fraction of accelerated particles are accumulated in the loop. Under flaring loop conditions, the trapping itself suggests that electrons are lacking within a loss cone, and therefore, they are distributed anisotropically (perpendicularly to magnetic field lines). Further and possibly the strongest evidence of the transverse anisotropy is the existence of the microwave loop-top brightness peak of optically thin gyrosynchrotron emission (Melnikov et al. 2001; Kundu et al. 2001), which has been interpreted as a tracer of a strong concentration of mildly relativistic electrons trapped and accumulated in the top of a flaring loop (Melnikov et al. 2002a). On the other hand, there are many observations of electron beams in the solar corona and flaring loops (Aschwanden et al. 1990). We should also mention the strong directivity of gamma-ray solar flares discovered from center-to-limb variations of their intensity

¹ Purple Mountain Observatory, National Astronomical Observatories, Nanjing 210008, China.

² Ioffe Institute for Physics and Technology, 194021 St. Petersburg, Russia.

³ New Jersey Institute of Technology, Newark, NJ 07102.

⁴ Radiophysical Research Institute (NIRFI), Nizhny Novgorod 603950, Russia.

(McTiernan & Petrosian 1991). Center-to-limb variations of microwave bursts are found as well (Silva & Valente 2002). On top of this, some acceleration processes result in anisotropic particle distributions (Miller et al. 1997; Pryadko & Petrosian 1999; Aschwanden 2002). Thus, nonisotropic pitch-angle distributions of fast electrons should be rather common. Nevertheless, most of the studies of the gyrosynchrotron emission neglect the effect of anisotropy, except for a few papers (e.g., Lee & Gary 2000; Lee, Gary, & Shibasaki 2000; Fleishman & Melnikov 2003).

Lee & Gary (2000) studied mainly the kinetics of electrons with initial anisotropy in the loop with account of magnetic mirroring and (weak) Coulomb scattering. The pitch-angle distribution of electrons was evolving with time, which resulted in spectral dynamics of the calculated microwave spectrum in the optically thin region. The model has been successfully applied for the analysis of a particular microwave burst (Lee et al. 2000), providing further evidence for particle anisotropy in solar flares.

Fleishman & Melnikov (2003) studied the effects of anisotropy on optically thick gyrosynchrotron emission and found the anisotropy to affect substantially both radiation spectra and polarization. In particular, the harmonic nature of gyrosynchrotron emission becomes more pronounced for the anisotropic case, providing more prominent spectral structure of the emission at low frequencies. Large (strongly polarized) narrow peaks arise frequently close to the lowest harmonics of the gyrofrequency.

The current paper concentrates on the proper effect of pitch-angle anisotropy on the whole spectrum, while particular attention is paid to the optically thin gyrosynchrotron emission. We found the anisotropy to have a strong effect on the intensity, polarization, and spectral index of the optically thin gyrosynchrotron emission. Evidently, this knowledge is important for diagnostics of particle and plasma parameters in flaring loops. The discovered effects relate primarily to the energy-dependent directivity (1) of the synchrotron radiation by a single electron.

Before discussing our numerical results, let us review briefly the current idea about gyrosynchrotron radiation produced by isotropic electron distributions with a power-law energy E (or momentum, p) spectrum. The frequency spectrum (J) of the radiation typically consists of optically thick (rising with frequency, f) and optically thin (falling with frequency) parts. The spectral maximum corresponds to the frequency defined by the condition

$$\tau(f) \sim 1, \quad (2)$$

where τ is the optical depth of the source. Alternatively, the spectral peak can be defined by the Razin effect (Razin 1960a), the peak frequency is close to the Razin frequency— $f_R = 2f_{pe}^2/3f_{Be}$ in this case—where f_{pe} is the electron plasma frequency and f_{Be} is the electron gyrofrequency. Both rising-with-frequency and falling-with-frequency parts of the spectrum are *optically thin* for this case.

The optically thin region at the frequencies above the Razin frequency is assumed to obey a power law,

$$J \propto f^{-\alpha}, \quad (3)$$

where α is the spectral index of the emission, which is specified by the spectral index δ in the electron energy distribution. In the ultrarelativistic approximation, we have

(Korchak & Terletsky 1952; Getmantsev 1952)

$$\alpha = \frac{\delta - 1}{2} \quad (4)$$

in some frequency range that depends on low-energy and high-energy cutoffs in the energy distribution of fast electrons (Korchak 1957; Syrovatsky 1959), while for the mildly relativistic case in the limits $10 < f/f_{Be} < 100$, the approximation proposed by Dulk & Marsh (1982) is frequently used,

$$\alpha = 0.90\delta - 1.22. \quad (5)$$

A better (nonlinear) approximation for this case was proposed by Zhou et al. (1998, 1999). We should note, however, that the exact formalism (Ramaty 1969) does not give a single spectral index. On the contrary, α changes continuously with frequency. At low frequencies ($f/f_{Be} < 20$), the index α increases remarkably, compared with equations (4) and (5), for tenuous plasma. On the other hand, if the plasma density in a source is high enough, the spectral index decreases in a rather wide optically thin region (Razin 1960b). These two reasons are shown to lead to considerable corrections when estimating δ from solar microwave observations (V. F. Melnikov et al. 2003, in preparation).

The emission of ultrarelativistic electrons is linearly polarized, so the degree of circular polarization is zero (Korchak & Syrovatsky 1961). However, in the mildly relativistic approach, the emission is mostly circularly polarized (Ramaty 1969; Takakura 1972). The sense of polarization corresponds to X -mode in the optically thin region and to O -mode in the optically thick region. The degree of polarization is large for small view angles (quasi-parallel to the magnetic field radiation) and small for large view angles (quasi-transverse radiation), respectively.

Most of these commonly accepted properties are subject to change for anisotropic pitch-angle distributions. The organization of the paper is as follows. Section 2 describes the model adopted for our calculations. Section 3 presents the results of the calculations through a broad range of the involved parameters. Section 4 discusses the discovered effects, their observability, and impact on current models of flaring microwave emission.

2. THE MODEL

Since our goal is to reveal the proper effect of the pitch-angle anisotropy on the gyrosynchrotron emission, we consider a uniform source with a constant magnetic field and time-independent distribution of fast electrons.

Thus, the radiation intensity of each wave mode is described by

$$J_\sigma(\omega, \vartheta) = \frac{j_\sigma(\omega, \vartheta)}{\kappa_\sigma(\omega, \vartheta)} (1 - e^{-\tau_\sigma}), \quad (6)$$

where $\tau_\sigma = \kappa_\sigma L$ is the optical depth of the source for either ordinary ($\sigma = 1$) or extraordinary ($\sigma = -1$) modes of radiation, L is the source size along the line of sight, $j_\sigma(\omega, \vartheta)$, $\kappa_\sigma(\omega, \vartheta)$ are the emissivity and absorption coefficient of the gyrosynchrotron emission at frequency ω and viewing angle ϑ . (Their expressions are given in the Appendix.)

The emissivity and the absorption coefficient were calculated by direct numerical integration with the Gaussian recipe (Abramovitz & Stegun 1964) and consequent summation of the series over n . Exact expressions of the Bessel functions were used (and recurrent relations for their derivatives).

The numerical calculations were performed (and the figures were plotted) for dimensionless values $j_\sigma^{\text{num}}(\omega, \vartheta)$, $\chi_\sigma^{\text{num}}(\omega, \vartheta)$, and $J_\sigma^{\text{num}}(\omega, \vartheta)$. The transition to the dimension values can be done according to the rules,

$$j_\sigma(\omega, \vartheta) = \frac{4\pi^2 e^2}{c} N_e \omega_{\text{Be}} j_\sigma^{\text{num}}(\omega, \vartheta), \quad (7)$$

$$\chi_\sigma(\omega, \vartheta) = \frac{\pi \omega_{\text{Be}} N_e}{2c N} \chi_\sigma^{\text{num}}(\omega, \vartheta), \quad (8)$$

$$J_\sigma(\omega, \vartheta) = 8\pi e^2 N J_\sigma^{\text{num}}(\omega, \vartheta), \quad (9)$$

where e is the electron charge, N_e and N are the number density of fast and background electrons, respectively, and ω_{Be} is the electron gyrofrequency. Accordingly, the optical depth is related to the dimensionless absorption coefficient $\chi_\sigma^{\text{num}}(\omega, \vartheta)$ by the formula

$$\tau_\sigma = \frac{\pi L \omega_{\text{Be}} N_e}{2c N} \chi_\sigma^{\text{num}}(\omega, \vartheta). \quad (10)$$

We assume the electron distribution function to have the form

$$f(\mathbf{p}) = \frac{N_e}{2\pi} f_1(p) f_2(\mu), \quad \int f(\mathbf{p}) p^2 dp d\mu d\varphi = N_e, \quad (11)$$

where $\mu = \cos \theta$ is the cosine of the particle pitch-angle and φ is the azimuth angle. The functions f_1 and f_2 are both normalized by unity,

$$\int f_1(p) p^2 dp = 1, \quad \int_{-1}^1 f_2(\mu) d\mu = 1. \quad (12)$$

All calculations were performed for a power-law distribution over momentum

$$f_1(p) = \frac{(\gamma - 3) p_0^{\gamma-3}}{p^\gamma}, \quad p_{\min} < p < p_{\max}, \quad (13)$$

with $p_{\min} = 0.2mc$ ($E_{\text{kin}} \approx 10$ keV) and $p_{\max} = 20mc$ ($E_{\text{kin}} \approx 10$ MeV). The normalization coefficient in equation (13) is calculated for a broad spectrum with $p_{\max} \gg p_{\min}$, which falls with increasing momentum. The spectral index γ relates to the energy spectral index δ as follows: $\gamma = 2\delta + 1$ for $E_{\text{kin}} \ll mc^2$ and $\gamma = \delta + 2$ for $E_{\text{kin}} \gg mc^2$. The angular distribution was modeled by either a function varying as a power of sine of the pitch angle, hereafter sin-N function (Hewitt, Melrose, & Rönmark 1982),

$$f_2(\mu) \propto \begin{cases} \sin^{-N} \left(\frac{\pi \theta}{2\theta_c} \right), & 0 < \theta < \theta_c, \\ 1, & \theta_c < \theta < \pi - \theta_c, \quad \mu = \cos \theta, \\ \sin^{-N} \left[\frac{\pi(\theta - \pi)}{2\theta_c} \right], & \pi - \theta_c < \theta < \pi, \end{cases} \quad (14)$$

or Gaussian function,

$$f_3(\mu) \propto \exp[-(\mu - \mu_1)^2 / \mu_0^2]. \quad (15)$$

The functions $f_2(\mu)$ and $f_3(\mu)$ with $\mu_1 = 0$ describe the pitch-angle distributions of the loss cone type with the transverse anisotropy of energetic electrons. The function $f_3(\mu)$ with $\mu_1 = 1$ describes the beamlike distribution of electrons propagating along the field lines.

The plotted values are the total intensity

$$J = J_X + J_O, \quad (16)$$

the degree of polarization

$$P(\omega, \vartheta) = \frac{J_X(\omega, \vartheta) - J_O(\omega, \vartheta)}{J_X(\omega, \vartheta) + J_O(\omega, \vartheta)}, \quad (17)$$

and the (local) spectral index

$$\alpha = \ln \left[\frac{J(\omega + \Delta\omega)}{J(\omega)} \right] / \ln \left[\frac{(\omega + \Delta\omega)}{\omega} \right] \\ = -\frac{\omega}{\Delta\omega} \ln \left[\frac{J(\omega + \Delta\omega)}{J(\omega)} \right], \quad (18)$$

where $\Delta\omega$ is the step in the ω -axes in our calculations. When generating the plots, the step in frequency was set as 3% of the frequency, which corresponds to the announced spectral resolution for the Frequency Agile Solar Radiotelescope (FASR; Bastian et al. 1998).

3. NUMERICAL RESULTS

To study the effect of pitch-angle anisotropy on gyro-synchrotron emission, we varied the type of pitch-angle distributions (loss cone-like and beamlike) and their parameters, such as the widths of the sin-N and Gaussian functions, θ_c , and μ_0 . The effects of these variations were considered for different involved parameters such as the electron spectral index γ and the parameter $\tau_0 - (\pi L \omega_{\text{Be}} / 2c)(N_e / N)$ that specifies the optical depth of the source as well as the plasma frequency to gyrofrequency ratio $Y = \omega_{\text{pe}} / \omega_{\text{Be}}$. The frequency dependences of intensity, degree of polarization, and spectral index of gyro-synchrotron emission were calculated for quasi-parallel and quasi-transverse wave propagation (angles between magnetic field vector and the line of sight $\vartheta = 37^\circ$ and $\vartheta = 78^\circ$, respectively). To be complete, we discuss below both new properties of gyro-synchrotron radiation directly related to the effect of pitch-angle anisotropy and some of the well-known properties valid for both isotropic and anisotropic distributions.

3.1. Pitch-Angle Distributions of sinN Type

We start with the anisotropy of the loss cone type described by sin-N function (eq. [14]) with $N = 6$. The size of the loss cone (parameter θ_c) varies from 0 (isotropic case) to $\pi/2$ (very wide loss cone: energetic electrons are distributed perpendicular to magnetic field).

General properties.—Let us consider a relatively soft electron spectrum ($\gamma = 9$) and tenuous plasma ($Y = 0.3$) with $\tau_0 = 5 \times 10^4$ (Fig. 1). The soft electron spectrum is more favorable to observe the spectral structure of the gyro-synchrotron radiation. The accepted parameter $Y = 0.3$ is chosen because larger values of Y produce a stronger effect of

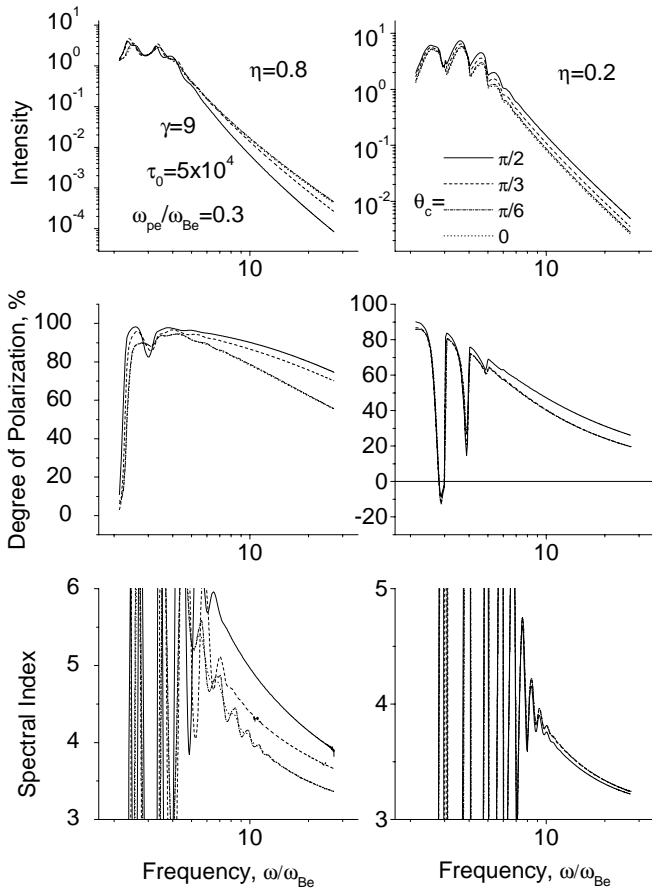


FIG. 1.—Gyrosynchrotron radiation intensity, degree of polarization, and spectral index vs. frequency for various loss cone angles θ_c in sin-N pitch-angle distribution. The decrease of intensity and increase of the degree of polarization and spectral index with θ_c are clearly seen for the quasi-parallel propagation ($\eta = 0.8$). The parameters are shown in the figure.

density, while smaller values are favorable to produce coherent electron cyclotron maser emission (Fleishman & Melnikov 1998) that is beyond the scope of this paper.

For the adopted set of parameters, the optical depth τ exceeds unity only at the lowest integer harmonics of the gyrofrequency (Fig. 1, *left panels*: $s = 2$; *right panels*: $s = 2, 3$).

In the quasi-parallel direction ($\eta = \cos \vartheta = 0.8$), the increase of anisotropy is followed by the strong decrease of intensity (up to a factor of 5–10) and an increase of polarization (up to 10%–20%) at high frequencies where the radio source is optically thin. The increase of the spectral index α is especially remarkable, $\Delta\alpha \sim 1$ (Fig. 1, *left column, bottom*). The curves for relatively large anisotropy ($\theta_c = \pi/3$, $\theta_c = \pi/2$) deviate clearly from the curves for the isotropic distribution and the weak anisotropy $\theta_c = \pi/6$ and show a considerable enhancement over the relativistic value $\alpha = (\delta - 1)/2 = (\gamma - 3)/2 = 3$ that is the asymptotic value for each curve for sufficiently high frequencies.

The physical reasons for such a behavior are as follows. The intensity of emission in the quasi-parallel direction at low frequencies is weakly sensitive to the pitch-angle anisotropy because the low-energy electrons contribute the bulk to the emitted energy at these frequencies. The emission by a single low-energy electron does not display prominent directivity; hence, the actual angular distribution is not so

important for the low-frequency emission. However, the directivity increases with the emitting electron energy, which results in a lack of higher frequency emission at small view angles ϑ from the loss cone distribution. The degree of polarization increases with the anisotropy, because O -mode emission at any given frequency is produced by electrons with higher energy than the respective X -mode emission. Accordingly, the directivity of O -mode emission is stronger than for X -mode, providing less favorable conditions for O -mode emission at quasi-parallel directions.

The emission properties in the quasi-transverse direction, $\eta = 0.2$ (Fig. 1, *right panels*), are not so sensitive to the loss cone type anisotropy, which agrees with the above one-electron consideration. The level of radiation intensity increases for the anisotropic distributions due to the excess of fast electrons moving quasi-transverse to the magnetic field directions compared with the isotropic case. The degree of polarization increases noticeably for a wide loss cone ($\theta_c = \pi/2$) only. The reason for this increase is that electrons from a wider range of pitch-angles contribute more to the X -mode intensity than to O -mode intensity (again, because the X -mode radiation is produced by lower energy electrons than the O -mode radiation). The decrease of the spectral index for the anisotropic case ($\theta_c = \pi/2$) is rather weak while present. The degree of polarization and the spectral index do not change unless the anisotropy is moderate ($\theta_c = \pi/6, \pi/3$) since the electrons described by the flat (independent of θ) region of the distribution (eq. [14]) contribute the bulk of the quasi-transverse wave emission.

One can note the wiggles in the spectra (Fig. 1, *top*) related to the harmonic structure of the gyrosynchrotron radiation that are clearly visible as oscillations of spectral index (Fig. 1, *bottom*). The oscillations are visible up to $\omega/\omega_{Be} \sim 10$, which might be used for the diagnostics of the magnetic field at the source. The number of oscillations depends on the anisotropy: the most oscillating curve (for $\eta = 0.8$, Fig. 1, *bottom left*) is for $\theta_c = \pi/6$ when the direction of emission is close to the direction of the fastest change of the distribution function with pitch angle ($\cos \theta_c \approx 0.87$ for $\theta_c = \pi/6$).

In general, the influence of the anisotropy on the emission properties in the optically thin region holds qualitatively the same for various parameters in the radio source, while variations of the electron spectral index, the optical thickness, or plasma density (the parameter $Y = \omega_p/\omega_B$) can, nevertheless, have an important effect on properties of the radiation.

Effect of the optical depth.—Generally, an increase of the optical depth produces a shift of the spectral peak toward higher frequencies for both isotropic and anisotropic cases. Figure 2 displays the gyrosynchrotron radiation for the same parameters as Figure 1, except τ_0 is increased by 4 orders of magnitude. The main effect of the large optical depth (for both isotropic and anisotropic cases) is a well-developed spectral peak at $\omega/\omega_{Be} \approx 10$. The harmonic structure is no longer dominating the transition from the optically thick to thin regions. The spectral index displays smooth curves with a well-developed maximum: the curves approach the relativistic value [$\alpha = (\gamma - 3)/2 = 3$] at higher frequencies.

The degree of polarization behaves similarly to that in Figure 1 in the optically thin region, while it corresponds mainly to O -mode in the thick region. This property relates primarily to the already mentioned difference in

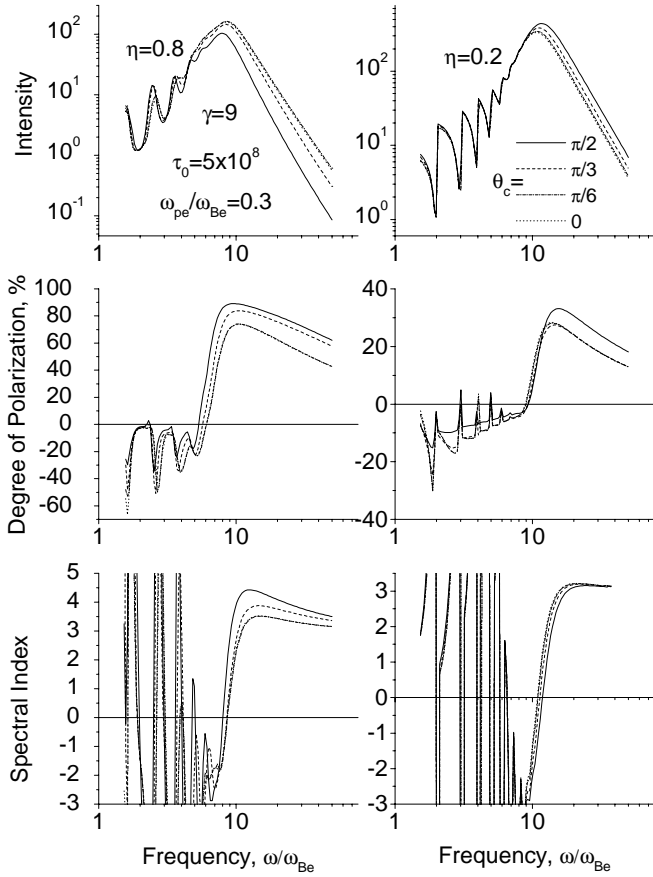


FIG. 2.—Same as in Fig. 1, but with the 4 order of magnitude higher optical thickness. The spectral index at high frequencies displays smooth curves with a well-developed maximum; the curves approach the relativistic value [$\alpha = (\gamma - 3)/2 = 3$] at higher frequencies. The degree of polarization corresponds mainly to O -mode in the optically thick region. The degree of O -polarization is weaker for the anisotropic case.

characteristic electron energy producing O - and X -mode emission at a given frequency. Since the level of radiation in the optically thick region can be qualitatively described in terms of effective temperature of radiating electrons, the brightness temperature of O -waves is larger than that of X -waves, providing the predominant O polarization that is well known for the isotropic case. The degree of O polarization becomes weaker for the anisotropic case because (as it has been explained above) the loss cone distribution is more favorable to produce X -waves than the isotropic distribution.

Effect of density.—The effect of density (namely, the role of wave dispersion in a medium) on the emission of electromagnetic waves by fast electrons was discovered in the early 1950s. In particular, Tsytoich (1951) studied the effect of density on emission in a medium with the refraction index $n > 1$. Ginzburg (1953) showed that the decrease of emissivity of the synchrotron radiation becomes important in dense plasmas ($n < 1$), while Ter-Mikaelyan (1954) examined the effect of density on the bremsstrahlung. If the plasma parameter Y is large ($Y \gg 1$), the density effect is known to provide the strong deformation of the synchrotron emission frequency spectrum (Razin effect), an exponential decrease of the emissivity and absorption coefficient at low frequencies, $f < f_R$ (Razin 1960a, 1960b), and considerable

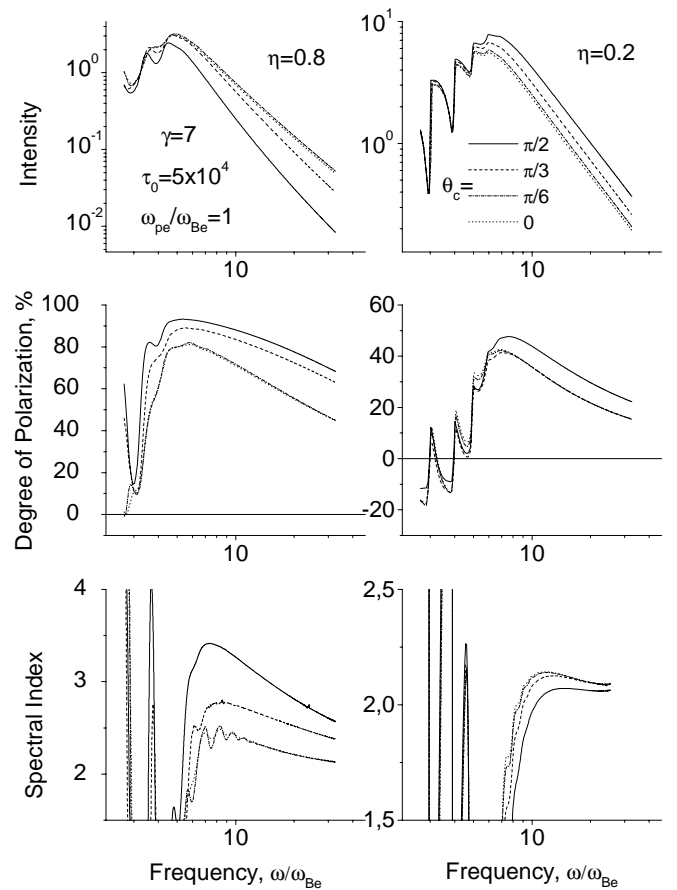


FIG. 3.—Same as in Fig. 1, but with the higher plasma density (parameter $Y = \omega_{pe}/\omega_{Be}$ increased from 0.3 to 1) and a harder electron spectrum.

flattening of the original synchrotron power-law spectrum, $F_f \sim f^{-\alpha}$, at higher frequencies (Razin 1960b).

Figure 3 displays the radiation for $Y = 1$ when the effect of density is not so strong and the main spectral peaks (for both quasi-parallel and quasi-transverse directions) are provided by the effect of optical depth. In particular, the degree of polarization decreases to the left from the spectral peak and can change the sense of polarization (Fig. 3, *middle right*). The spectral index has a maximum and approaches the relativistic value ($\alpha = 2$) from above. The oscillations of spectral index occur for the favorable anisotropy ($\theta_c = \pi/6$) as in Figure 1 (*bottom left*). The oscillations appear to be weaker in Figure 3 than in Figure 1, which is an effect of both increased density and decreased electron spectral index γ (see next subsection as well).

For the larger plasma parameter (Fig. 4; $Y = 3$), the effect of optical depth is much less important. (To emphasize this, we even increased the τ_0 value a bit compared with Fig. 3.) For the quasi-parallel wave emission, the spectral peak is entirely provided by the effect of density. There appears a region of rapid decrease of the intensity at the low frequencies, $\omega < \omega_R \approx 6\omega_{Be}$. The peak intensity is 1 order of magnitude less here than in Figure 3.

The degree of polarization is not decreasing to the left from the spectral peak, while it keeps growing as the frequency is decreasing. This means that the effect of density suppresses the O -mode radiation more effectively than the X -mode radiation. The degree of polarization is

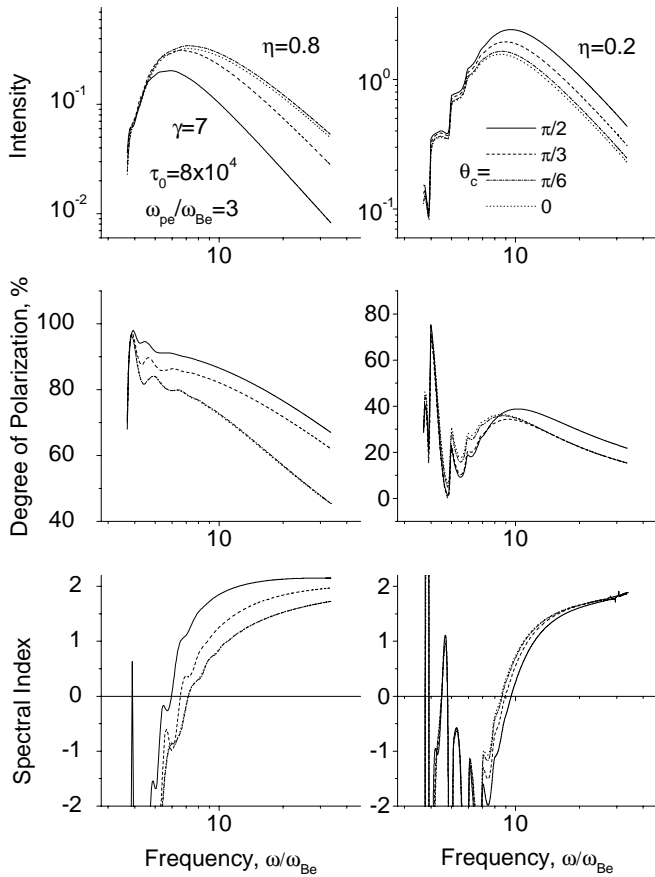


FIG. 4.—Same as in Fig. 3, but for denser plasma. For the quasi-parallel wave emission, the spectral peak is entirely provided by the Razin effect. The degree of polarization is not decreasing to the left from the spectral peak, while it keeps growing as the frequency decreases. Both the degree of polarization and the spectral index are systematically stronger for the anisotropic distributions than for the isotropic one. The spectral index has no maximum anymore (cf. Fig. 3), while it approaches the relativistic value ($\alpha = 2$) from below.

systematically stronger for the anisotropic distribution than for the isotropic one.

The behavior of the spectral index is qualitatively different from that in Figure 3 (*bottom*): it has no maximum anymore, while it approaches the relativistic value ($\alpha = 2$) from below. In particular, the curves for the anisotropic distributions (*bottom left*) approach the relativistic value faster than the curve for the isotropic case, opposite to what we have in Figure 3 (*bottom left*). The common feature in these two figures is that the spectral index for an anisotropic distribution is larger than one for the isotropic distribution at any given frequency, i.e., the stronger the anisotropy, the steeper the frequency spectrum.

For the quasi-transverse wave emission (Fig. 4, *right column*), the effect of optical depth is noticeable: the degree of polarization decreases as frequency decreases at $\omega/\omega_{Be} = 6-10$. The density effect dominates even lower frequencies (e.g., the degree of polarization increases again). However, there is no well-established exponential decrease of the intensity spectrum, which could have been referred to as Razin suppression.

The Razin effect, operating together with the effect of the optical depth, is quite visible in Figure 5 (*left column*). The spectral peaks (at $\omega/\omega_{Be} = 20-30$) are provided primarily by

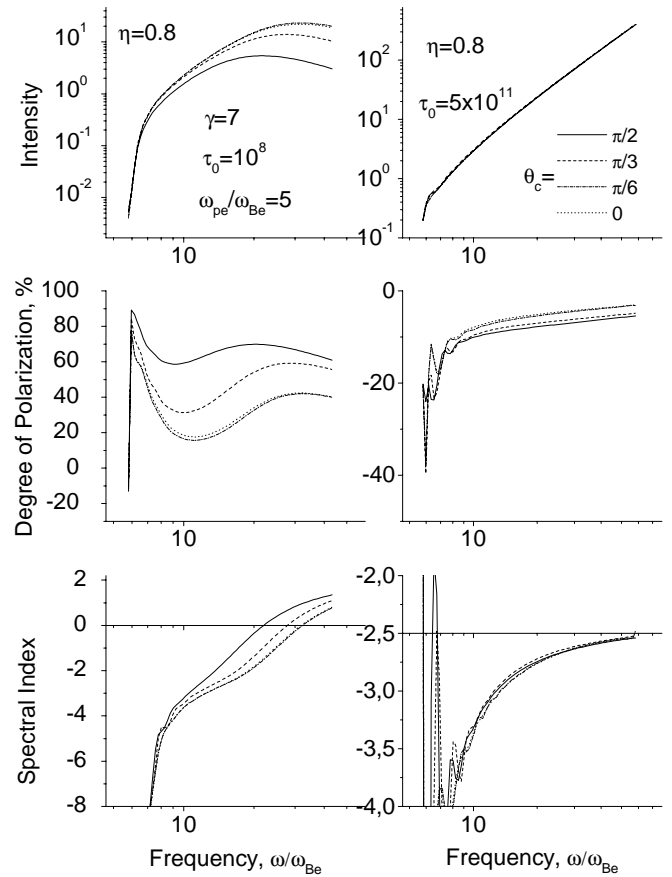


FIG. 5.—*Left column*: Razin effect and the effect of high optical depth operating together. Note the stronger X -mode polarization for the higher anisotropy. *Right column*: Extremely large optical depth. Anisotropy has no effect on the radiation intensity and has a weak effect on the degree of polarization and spectral index. Note the dependence of the spectral index on the frequency: the optically thick gyrosynchrotron radiation does not display any evident power law.

the effect of optical depth, while the effect of density is important as well. (The Razin frequency is $\omega_R \approx 17\omega_{Be}$.) It is the effect of density that keeps the degree of polarization positive in the optically thick region since it suppresses the O -mode radiation better than the X -mode radiation. For the anisotropic distributions, the degree of polarization can be rather large ($>60\%$); for the isotropic case, it is less than 40% .

At the frequencies less than the Razin frequency ($\omega < 17\omega_{Be}$ for this case), both the emissivity and the absorption coefficient have exponentially small factors. Nevertheless, until $\tau > 1$, the radiation intensity decreases slowly toward low frequencies because the intensity is specified by the ratio $j_\sigma/\chi\sigma$ here according to equation (6), and the exponentially small factors annihilate. However, as soon as τ decreases below unity due to the Razin suppression, the radiation intensity starts to drop exponentially (at $\omega < 8\omega_{Be}$ for the chosen set of parameters). In particular, the degree of polarization starts to grow (because O radiation is more suppressed by the Razin effect than X -radiation is), and the spectral index decreases drastically at these frequencies.

Figure 5 (*right*) displays the case of extremely large optical depth (parameter $\tau_0 = 5 \times 10^{11}$). Anisotropy has no effect on the radiation intensity and has a weak effect on the degree of polarization, which agrees well with the results of

Fleishman & Melnikov (2003): optically thick gyrosynchrotron radiation is weakly sensitive to the electron pitch-angle anisotropy for the case of a dense plasma. We should emphasize the dependence of the spectral index on the frequency. The optically thick gyrosynchrotron radiation does not display any evident power law approaching the relativistic asymptotics ($\sim \omega^{2.5}$) at very high frequencies only ($\omega > 50\omega_{Be}$). It is obviously correct for both isotropic and anisotropic distributions.

The effect of density is noticeable even for moderate Y values when there is no clear suppression of the low-frequency radiation, which is illustrated by Figure 6. The left and right columns have the only difference in Y value: $Y = 1$ for the left column and $Y = 2$ for the right column. The density effect provides the following changes in the radiation: (1) the optically thick part becomes smoother, (2) the X -mode degree of polarization becomes larger in the optically thick region, the sense of polarization can correspond to X -mode for the anisotropic case, while for O -mode for the isotropic case (Fig. 6, *middle right*), and (3) the region of the spectral peak becomes broader (the spectral index exceeds the zero level slower).

The behavior of the spectral index depends on the anisotropy. It approaches the relativistic value ($\alpha = 1$) from

below for the isotropic case, from above for an anisotropic case. Note that the position of the spectral maximum ($\alpha = 0$) depends on the pitch-angle anisotropy as well. The peak frequency (f_{peak}) decreases when the anisotropy increases. For the tenuous plasma, this effect is not so pronounced (compare with Fig. 2).

Effect of the electron spectral index.—Let us compare the left columns of Figure 3 and Figure 6. The only difference in the respective parameters is the γ values adopted for these two figures ($\gamma = 7$ in Fig. 3 and $\gamma = 5$ in Fig. 6). The following changes are evident as the hardness of the electron spectrum increases: the peak value of the intensity increases, the shape of the spectrum becomes smoother (no oscillations of the radiation spectral index are present in the optically thin region), and the radiation spectral index approaches the relativistic value [$\alpha = (\gamma - 3)/2$] faster. These properties hold for both isotropic and anisotropic distributions and can be easily understood since the effect of the electron spectral index γ is provided primarily by the fact that the contribution of high-energy electrons becomes more important for harder electron spectra (smaller γ). The effect of anisotropy is similar for these two cases. The difference in spectral indices between the anisotropic and isotropic cases (at the same frequency) can be about $\Delta\alpha \approx 1$ for both Figure 3 and Figure 6.

If we compare these plots with Figure 1 for even softer electron distribution ($\gamma = 9$; the difference in Y is not so important. The only effect of a small Y value in Fig. 1 is the enhanced low-frequency radiation due to the contribution of low-energy electrons, which is suppressed in Figs. 3 and 6), we find the same systematics.

3.2. Effect of Pitch-Angle Distribution Shape: Gaussian Loss Cone

Properties of gyrosynchrotron radiation have exceedingly strong dependence on the functional shape of the pitch-angle distribution of the loss cone type. To illustrate this, we now assume the distribution obeys equation (15) with $\mu_1 = 0$ and vary the parameter μ_0 from 0.2 to 10 (from narrow, pancake-like to almost isotropic distribution).

Figure 7 displays the plots for relatively tenuous plasma, $Y = 0.5$. The radiation intensity changes by orders of magnitude compared with the isotropic case. In particular, the difference in the spectral index in the optically thin frequency range is up to a factor of 4 (*left panel, bottom*). A remarkable change of polarization occurs as well. The degree of polarization increases in the optically thin region for all view angles: it can exceed 50% for quasi-transverse directions and reach 100% for quasi-parallel directions. Furthermore, the sense of polarization can correspond to X -mode in the optically thick region.

The effects hold for denser plasma also. Figure 8 displays the plots for $Y = 2$. Generally, the spectral peak moves toward higher frequencies as Y increases. Therefore, we reduced the value of τ_0 a little to keep the spectral peak at approximately the same position as in Figure 7. The optically thin region does not change much compared with that in Figure 7, while the spectrum in the optically thick region becomes smoother for denser plasma since the contribution of low-energy electrons is suppressed by the effect of density. One can also note that the region of the spectral peak becomes a bit broader for denser plasma for both isotropic and anisotropic cases, which is similar to what we have for

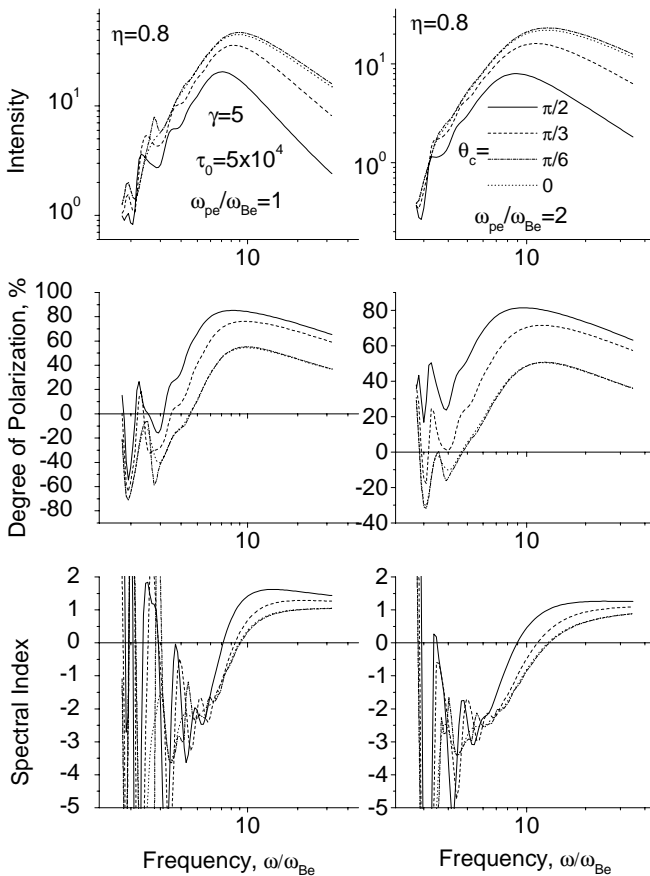


FIG. 6.—Illustration of the density effect on the emission parameters for the moderate values of Y . Note that for the higher parameter Y , the X -mode degree of polarization becomes larger in the optically thick region and the sense of polarization can correspond to X -mode for the anisotropic case, while for O -mode for the isotropic case. Note as well that the peak frequency f_{peak} decreases remarkably when the anisotropy increases. For the tenuous plasma, this effect is not so pronounced (cf. Fig. 2).

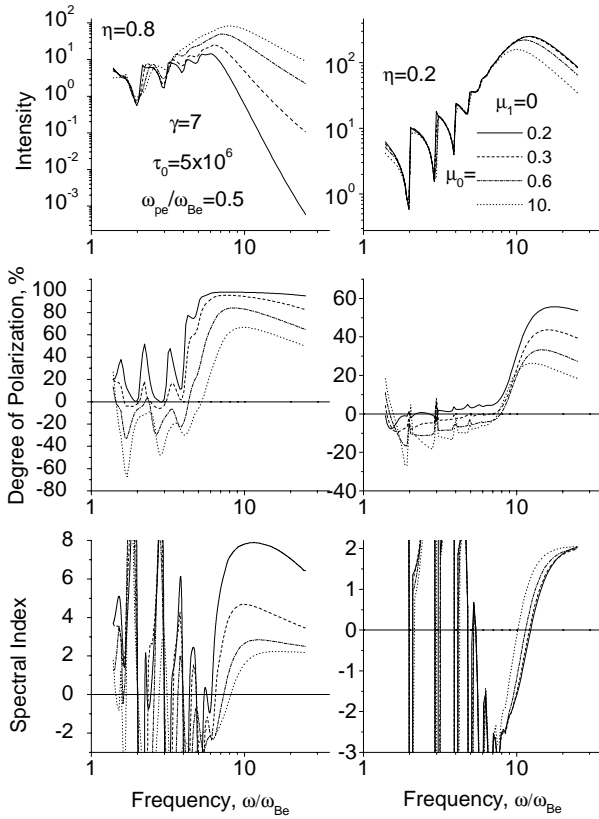


FIG. 7.—Gyrosynchrotron radiation intensity, degree of polarization, and spectral index vs. frequency for various μ_0 in the Gaussian pitch-angle distribution $f_3(\mu) \propto \exp[-(\mu - \mu_1)^2/\mu_0^2]$ of the loss cone type ($\mu_1 = 0$). Much stronger dependence on the anisotropy compared with the sin-N pitch-angle distribution is clearly seen.

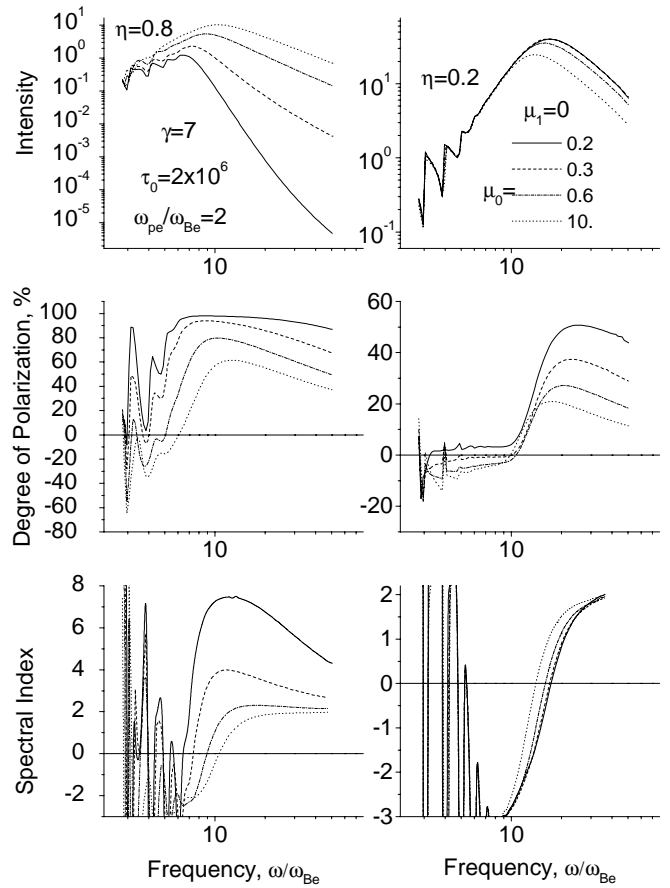


FIG. 8.—Same as in Fig. 7 for a denser plasma (parameter $Y = 2$)

sin-N pitch-angle distribution. Note also that the degree of polarization of the X-mode in the optically thick region increases remarkably compared with the case of tenuous plasma in Figure 7.

The exact results depend on the electron spectral index γ . For the same parameters as in Figures 7 and 8 and $\gamma = 9$, we found that the spectral index starts to oscillate around the position of the spectral peak. The oscillations become more prominent for smaller τ_0 values than in Figures 7 and 8, which are evident from Figure 9. (The Y value is set as 1 to be between 0.5 and 2 adopted for Figs. 7 and 8, respectively. The variations of Y value within these limits make no important difference.) For this case, the X-mode polarization varies with frequency between 0% and 100% in the optically thick region. The oscillating behavior of the spectral index in the optically thin region is clearly evident for both quasi-parallel and quasi-transverse directions. The stronger the anisotropy, the more pronounced the oscillations of the spectral index for the quasi-parallel wave emission (Fig. 9, bottom left), which is different from the behavior for sin-N distribution (Figs. 1 and 3, bottom left), where a moderate anisotropy (with $\theta_c = \pi/6$) produces the most oscillating spectral index.

Thus, the properties of gyrosynchrotron emission depend substantially on the shape of angular function describing the loss cone. We can see from Figures 1–9 that Gaussian anisotropy affects the emission much more than the aniso-

tropy of sin-N type. This is provided by a faster decrease in the number of electrons in the loss cone for the Gaussian case than for the sin-N case. Generally, for other equal conditions, the loss cone distributions are more favorable to produce X-mode radiation compared with the isotropic distribution.

3.3. Effect of Pitch-Angle Distribution Shape: Beamlike Distribution

Let us turn to the analysis of gyrosynchrotron emission produced by a beamlike electron distribution. For this purpose, we use the Gaussian distribution (eq. [15]) with $\mu_1 = 1$.

Figure 10 displays the plots for the view angles in the half-sphere of the beam propagation. Obviously, the beaming enhances the emission intensity along the beam ($\eta = 0.8$). The scatter of the spectral indices for various beam sizes (μ_0) is not too large while present. However, we should mention a significant decrease of the degree of polarization in the quasi-parallel direction. While for the isotropic case it exceeds 50%, it can be less than 30% for the anisotropic case—an unusual value for quasi-parallel directions.

The effect of the beamlike anisotropy on polarization appears to be much more prominent for quasi-transverse directions: the dominant sense of polarization is O-mode here for both optically thick and thin regimes. The sense of polarization changes its sign in the optically thin region from the X-mode to the O-mode with increasing anisotropy.

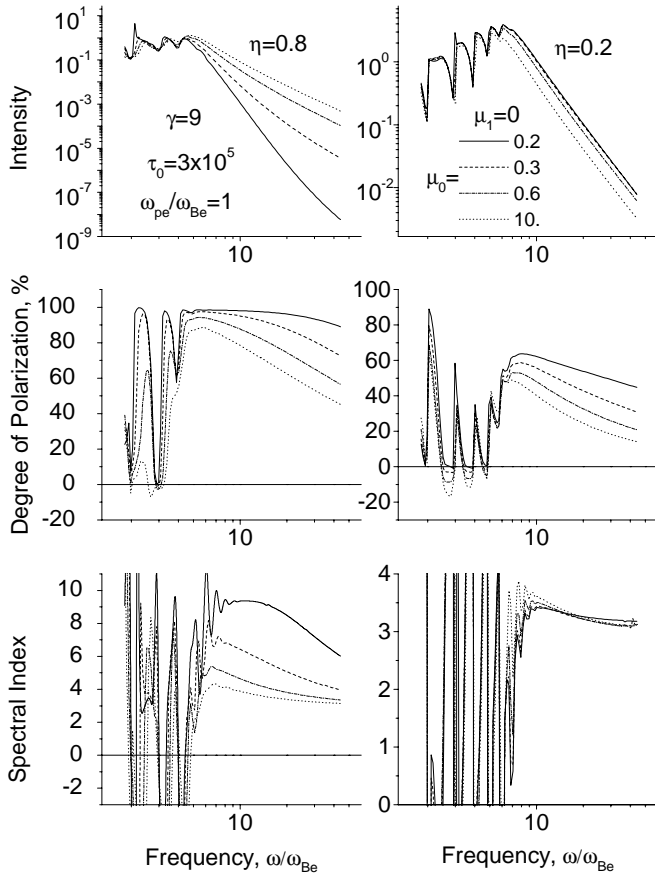


FIG. 9.—Same as in Fig. 7, but for the softer electron energy spectrum (spectral index $\gamma = 9$).

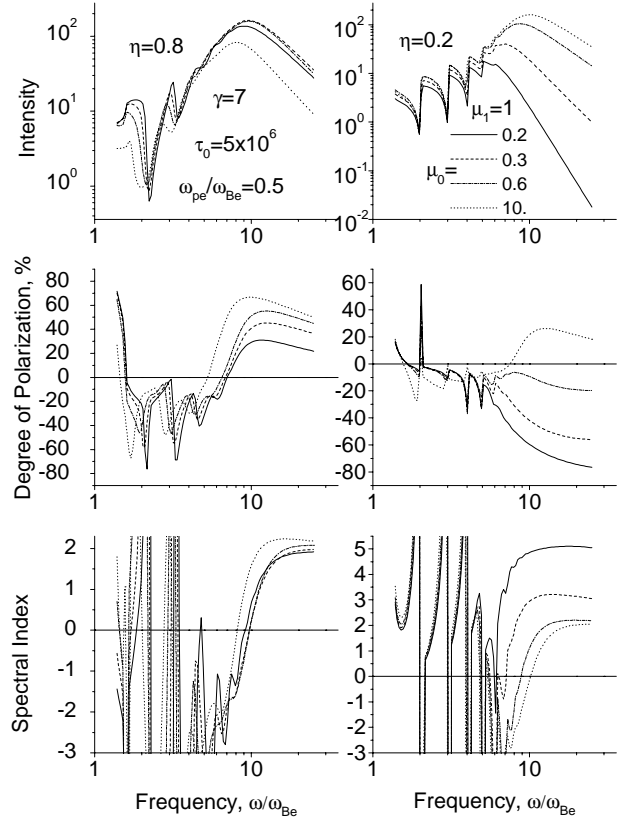


FIG. 10.—Gyrosynchrotron radiation intensity, degree of polarization and spectral index vs. frequency for various μ_0 in the Gaussian $f_3(\mu) \propto \exp[-(\mu - \mu_1)^2/\mu_0^2]$ pitch-angle distribution of the beamlike type ($\mu_1 = 1$). The influence of the anisotropy is especially well seen for the quasi-transverse propagation (*right column*). Beamlike distributions are more favorable to produce *O*-mode gyrosynchrotron emission even in the optically thin region.

Thus, beamlike distributions are more favorable to produce *O*-mode gyrosynchrotron emission, even in the optically thin region. This happens for all view angles in this half-sphere (Fig. 11). We should note that the sense of polarization can change with frequency in the optically thin region.

In the other half-sphere, counter to the direction of the beam propagation, the situation is opposite: strong *X*-mode polarization is observed here for all view angles (Fig. 12). An extremely large scatter of spectral indices takes place for this case. It is commonly accepted that large spectral indices ($\alpha > 8$) are a signature of gyrosynchrotron radiation produced by thermal electrons (Dulk & Marsh 1982). However, Figure 12 demonstrates that anisotropic nonthermal distributions can produce much softer gyrosynchrotron spectra.

Figure 13 displays the gyrosynchrotron emission by the beam in a dense plasma ($Y = 2.5$) when the optical depth is relatively large. The behavior of the polarization and the spectral index is generally the same as in Figure 10. However, we should note that even a rather broad optically thick region of the spectrum does not obey any single power law: the plots of the spectral index do not contain any flat negative part. This property has already been mentioned above for the loss cone and isotropic distributions.

Figure 14 plots the curves for different types of the Gaussian anisotropy: loss cone ($\mu_1 = 0$), beam ($\mu_1 = 1$), and the oblique beams ($\mu_1 = 0.3, 0.6$). From the figure, we conclude that a gradual transition occurs from the loss cone to the beamlike regime.

4. DISCUSSION

Our study proves the pitch-angle anisotropy significantly affects the gyrosynchrotron radiation. First of all, we should mention the strong effect of the anisotropy on the intensity and spectral index of the emission in the optically thin region, which relates primarily to the energy-dependent directivity (eq. [1]) of the synchrotron radiation by a single electron.

So far, the spectral index has been commonly believed to be directly linked to the energy spectral index of radiating electrons, providing the method of deriving the electron distribution from the microwave spectra (Bastian et al. 1998). However, this method cannot be applied directly if the radiating electrons have an anisotropic pitch-angle distribution since the value of the spectral index can deviate significantly from the respective value for the isotropic case. Nevertheless, the results are potentially even more powerful for the fast particles diagnostics if applied for the analysis of spectral index distribution along the magnetic loop obtained with high spectral and spatial resolution, which should become possible for the planned FASR observations (Bastian et al. 1998). Furthermore, the oscillating behavior of the spectral index can be used for magnetic field diagnostics.

Currently, it is known that with the Nobeyama radio-heliograph data, microwave emission from the footprint

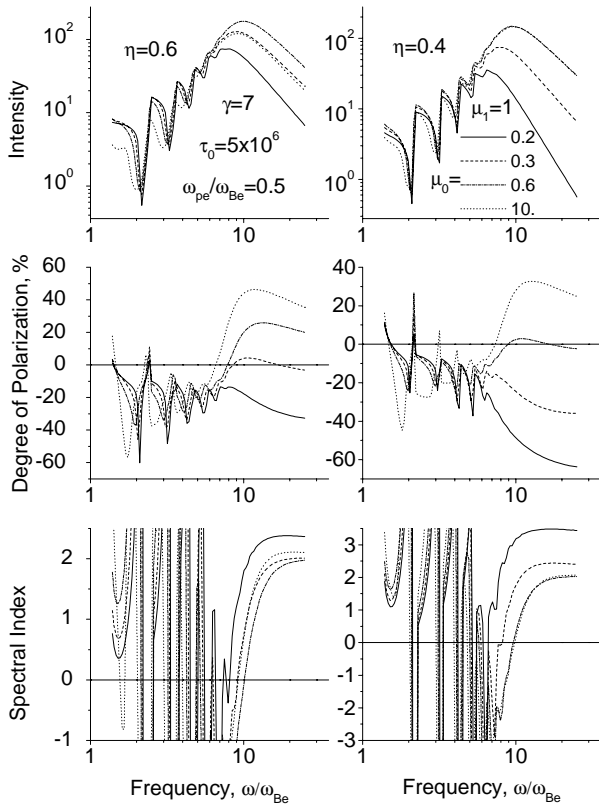


FIG. 11.—Same as in Fig. 10, but for different propagation angles ($\eta = 0.6$ and $\eta = 0.4$). Note that the sense of polarization can change with frequency in the optically thin region.

parts of extended flaring loops displays systematically softer spectra ($\Delta\alpha \sim 1\text{--}1.5$ in the domain 17–34 GHz) than from the loop-top part (Yokoyama et al. 2002; Melnikov et al. 2002b). It has been shown that one of the reasons for the spectral softening is the systematic increase of the magnetic field strength from the loop top toward the footpoints. Accordingly, the emission at a given frequency is generated at lower gyroharmonics for the footpoints than for the loop-top, which can result in softer footpoint spectra (see, e.g., Fig. 1) with $\Delta\alpha \sim 0.5\text{--}1$ (V. F. Melnikov et al. 2003, in preparation).

The results presented in the paper show clearly that a pitch-angle anisotropy can make an important contribution to the observed spectral index variations. Indeed, if we take into account the mentioned convergence of the magnetic field lines toward the footpoints, we should expect a more anisotropic electron distribution (due to a larger loss cone) in the footpoint source than in the loop-top source. Furthermore, for the disc flares, the footpoint source is observed at a quasi-parallel direction, while the loop-top source is observed at a quasi-transverse direction. Figures 1–4 and Figures 7–9 show that anisotropic distributions provide *systematically* softer spectra of gyro-synchrotron radiation (at quasi-parallel directions, in the case of the footpoint source) than the isotropic or weakly anisotropic distribution (at quasi-transverse directions, in the case of the loop-top source), which agrees with the Nobeyama radioheliograph data. Thus, the pitch-angle anisotropy probably plays a key role in the observed variations of the spectral index of the microwave radiation along the loop.

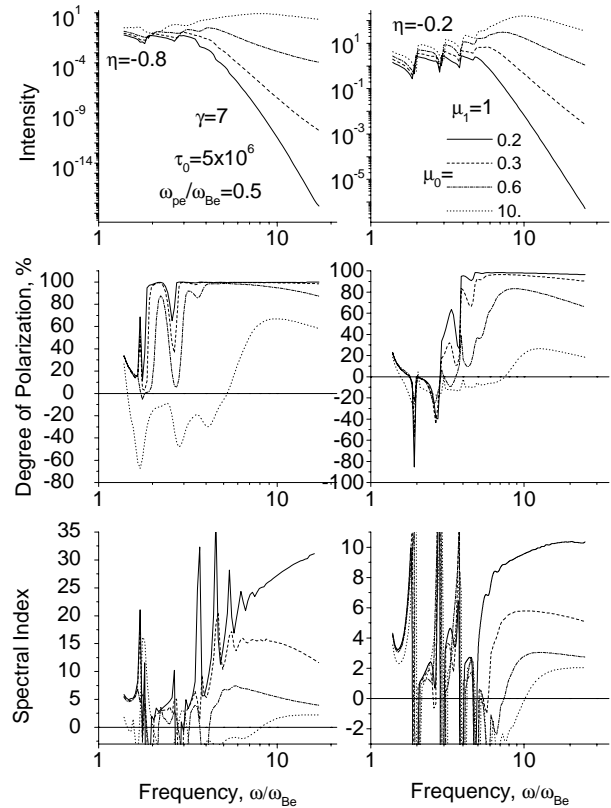


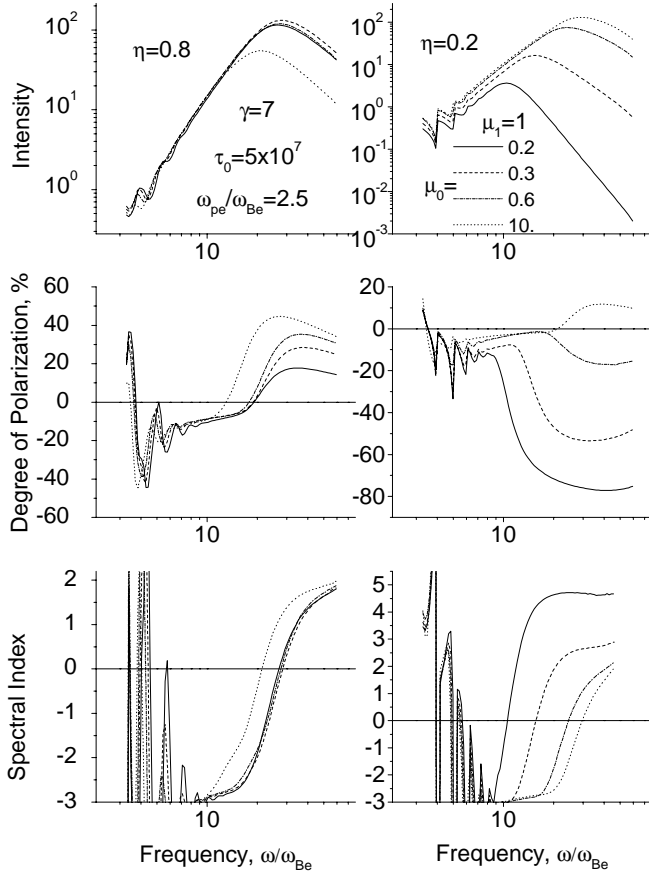
FIG. 12.—Same as in Fig. 10, but for the half-sphere opposite to the direction of the beam propagation. The dependence of the spectral index on anisotropy is very strong for this case: the value of α can increase by a factor of 10 as the anisotropy increases. The frequency spectrum can become extremely soft for beamlike pitch-angle distributions.

We should note as well that the decrease of the radiation intensity in the quasi-parallel direction due to the pitch-angle anisotropy is rather significant in explaining the observed decrease of the radio brightness from the loop-top to the footpoints of the flaring loops near the center of the solar disc (Melnikov et al. 2002a).

Actually, the study of gyrosynchrotron intensity and spectral index distribution together with hard X-ray and gamma-ray data from the *Ramaty High-Energy Solar Spectroscopic Imager (RHESSI)* mission can provide us with entirely new powerful tool to study pitch-angle distributions of fast electrons along the loop. Such information is of primary importance for the models of fast electron propagation in the magnetic loops since it can put essential constraints on the mirror ratio, background number density, level, and spectra of wave turbulence in the loop, which (all together) control the particle kinetics in the magnetic loop.

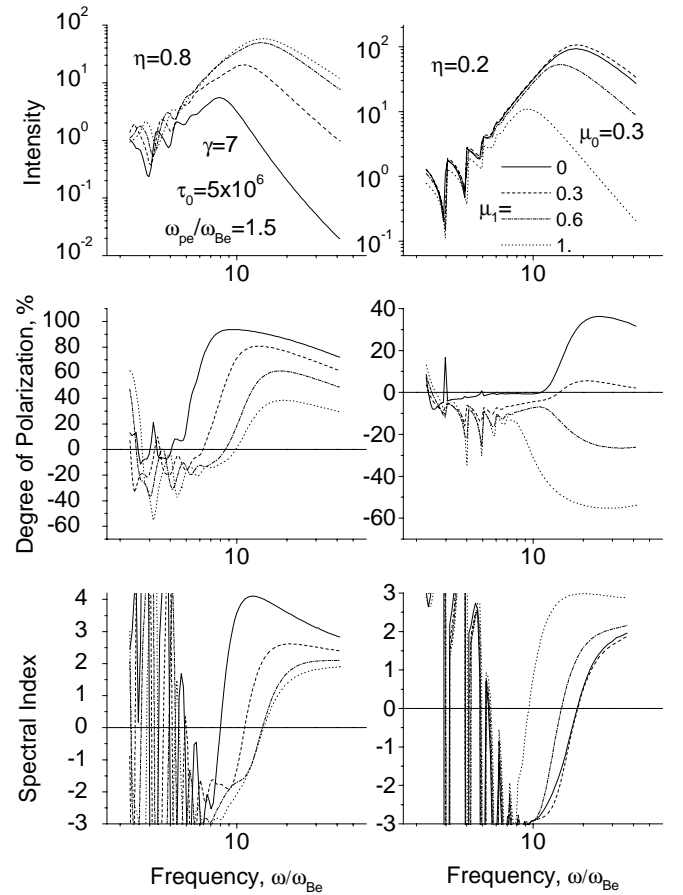
Furthermore, the properties of polarization can be used for diagnostic purposes as well. The anisotropic distributions can ensure *X*-mode polarization in the optically thick region or (in some cases, for beamlike distributions) *O*-mode radiation in the optically thin region. Multiple changes of the sense of polarization with frequency can occur. The degree of polarization can deviate extensively from the respective isotropic case.

We conclude that most of the effects found here can be observed (and some of them have already been observed); thus, detailed and careful interpretation of the micro-

FIG. 13.—Same as in Fig. 10, but for denser plasma ($Y = 2.5$)

wave data with the use of the presented results should substantially improve particle diagnostics and provide us with essentially new observational constraints on fast particle pitch-angle anisotropy in solar flares.

This work was supported by the Russian Foundation for Basic Research grants 00-02-16356, 01-02-16586, and 02-02-39005, Russian Federal Program: Astronomy,

FIG. 14.—Gyrosynchrotron radiation intensity, degree of polarization, and spectral index vs. frequency for different types of the Gaussian anisotropy: the loss cone ($\mu_1 = 0$), beam ($\mu_1 = 1$), and the oblique beams ($\mu_1 = 0.3, 0.6$).

Chinese NFS project 19833050, the 973 program with G2000078403, and NSF grant AST 99-87366 to the New Jersey Institute of Technology. V. M. is grateful to the National Astronomical Observatory of Japan for the support of his visit to NRO.

APPENDIX

The emissivity and self-absorption coefficient have the form (Eidman 1958, 1959; Ramaty 1969)

$$j_{\sigma}(\omega, \vartheta) = \frac{4\pi^2 e^2 \omega^2 [\partial(\omega n_{\sigma})/\partial\omega]}{c (1 + K_{\sigma}^2 + \Gamma_{\sigma}^2)} \sum_{n=1}^{\infty} \int \gamma_e \beta^2 d^3 p (1 - \mu^2) f(\mathbf{p}) \left[\frac{\Gamma_{\sigma} \sqrt{1 - \eta^2} + K_{\sigma} (\eta - \beta \mu n_{\sigma})}{n_{\sigma} \beta \sqrt{(1 - \mu^2)(1 - \eta^2)}} J_n(z) + J'_n(z) \right]^2 \times \delta(\gamma_e \omega - n \omega_{Be} - \gamma_e \beta n_{\sigma} \eta \mu \omega), \quad (\text{A1})$$

$$\kappa_{\sigma}(\omega, \vartheta) = - \frac{\pi \omega_{pe}^2}{(1 + K_{\sigma}^2 + \Gamma_{\sigma}^2) \{2n_{\sigma} [\partial(\omega n_{\sigma})/\partial\omega]\} v_{\sigma} N} \sum_{n=1}^{\infty} \int d^3 p (1 - \mu^2) \left[\frac{\Gamma_{\sigma} \sqrt{1 - \eta^2} + K_{\sigma} (\eta - \beta \mu n_{\sigma})}{n_{\sigma} \beta \sqrt{(1 - \mu^2)(1 - \eta^2)}} J_n(z) + J'_n(z) \right]^2 \times \delta(\gamma_e \omega - n \omega_{Be} - \gamma_e \beta n_{\sigma} \eta \mu \omega) \left[p \frac{\partial}{\partial p} - (\mu - n_{\sigma} \beta \eta) \frac{\partial}{\partial \mu} \right] f(\mathbf{p}) \quad (\text{A2})$$

where $f(\mathbf{p})$ is the distribution function (eq. [11]) of fast electrons, ω_{pe} and ω_{Be} are the electron plasma and gyrofrequencies, N is the number density of the background plasma, $\eta = \cos \vartheta$, ϑ is the view angle, $J_n(z)$ and $J'_n(z)$ are the Bessel function and its derivative over argument z , $z = (\omega/\omega_{Be}) \gamma_e n_{\sigma} \beta [(1 - \mu^2)(1 - \eta^2)]^{1/2}$, $\beta = v/c$ is the dimensionless particle velocity, v_{σ} is the group velocity of the σ -mode wave.

The polarization vector $e_{\sigma,\kappa}$ of σ -mode wave ($\sigma = 1$ for O -mode and $\sigma = -1$ for X -mode) in the reference frame with z -axes along the magnetic field \mathbf{B} and κ -vector in the (y, z) plane is

$$e_{\sigma,\kappa} = \frac{(1, i\alpha_\sigma, i\beta_\sigma)}{(1 + \alpha_\sigma^2 + \beta_\sigma^2)^{1/2}}, \quad (\text{A3})$$

where

$$\alpha_\sigma = K_\sigma \cos \theta - \Gamma_\sigma \sin \theta, \quad \beta_\sigma = K_\sigma \sin \theta + \Gamma_\sigma \cos \theta, \quad (\text{A4})$$

$$K_\sigma = \frac{2\sqrt{u}(1-v)\cos\theta}{u\sin^2\theta - \sigma[u^2\sin^4\theta + 4u(1-v)^2\cos^2\theta]^{1/2}}, \quad K_X K_O = -1, \quad (\text{A5})$$

$$\Gamma_\sigma = -\frac{v\sqrt{u}\sin\theta + uK_\sigma\cos\theta\sin\theta}{1-u-v(1-u\cos^2\theta)}, \quad (\text{A6})$$

$$v = \omega_{pe}^2/\omega^2, \quad u = \omega_{Be}^2/\omega^2. \quad (\text{A7})$$

The refractive indices have the form

$$n_\sigma^2 = 1 - \frac{2v(1-v)}{2(1-v) - u\sin^2\theta + \sigma[u^2\sin^4\theta + 4u(1-v)^2\cos^2\theta]^{1/2}} \quad (\text{A8})$$

Before doing the numerical calculations, the integrals over the azimuth angle ϕ and over μ in equations (A1) and (A2) were taken analytically (with the use of δ function). After the integration we have

$$j_\sigma(\omega, \vartheta) = \frac{8\pi^3 e^2}{cn_\sigma|\eta|} \frac{\omega[\partial(\omega n_\sigma)/\partial\omega]}{(1 + K_\sigma^2 + \Gamma_\sigma^2)} \sum_{n=1}^{\infty} \int \beta p^2 dp (1 - \mu^2) f(\mathbf{p}) \left[\frac{\Gamma_\sigma \sqrt{1 - \eta^2} + K_\sigma(\eta - \beta\mu n_\sigma)}{n_\sigma \beta \sqrt{(1 - \mu^2)(1 - \eta^2)}} J_n(z) + J'_n(z) \right] \Big|_{\mu=\mu_*}, \quad (\text{A9})$$

$$\begin{aligned} \kappa_\sigma(\omega, \vartheta) = & -\frac{\pi^2 \omega_{pe}^2}{\omega|\eta|v_\sigma N(1 + K_\sigma^2 + \Gamma_\sigma^2)} \{n_\sigma^2[\partial(\omega n_\sigma)/\partial\omega]\} \sum_{n=1}^{\infty} \int \frac{p^2}{\gamma_e \beta} dp (1 - \mu^2) \left[\frac{\Gamma_\sigma \sqrt{1 - \eta^2} + K_\sigma(\eta - \beta\mu n_\sigma)}{n_\sigma \beta \sqrt{(1 - \mu^2)(1 - \eta^2)}} J_n(z) + J'_n(z) \right]^2 \\ & \times \left[p \frac{\partial}{\partial p} - (\mu - n_\sigma \beta \eta) \frac{\partial}{\partial \mu} \right] f(\mathbf{p}) \Big|_{\mu=\mu_*}, \end{aligned} \quad (\text{A10})$$

where

$$\mu_* = \frac{\gamma_e \omega - n\omega_{Be}}{\gamma_e \beta n_\sigma \eta \omega}, \quad |\mu_*| \leq 1. \quad (\text{A11})$$

The respective dimensionless values (the normalization is described in the main text in eqs. [7] and [8]) were calculated numerically after substituting the distribution function (eq. [11]) of fast electrons.

REFERENCES

- Abramovitz, M., & Stegun, I. A. 1964, Handbook of Mathematical Functions (Boulder: Natl. Bureau of Standards)
- Alfvén, N., & Herlofson, N. 1950, Phys. Rev., 78, 616
- Aschwanden, M. J. 2002, Space Sci. Rev., 101, 1
- Aschwanden, M. J., Benz, A. O., Schwartz, R. A., Lin, R., Pelling, R. M., & Stehling, W. 1990, Sol. Phys., 130, 39
- Bastian, T. S., Benz, A. O., & Gary, D. E. 1998, ARA&A, 36, 131
- Bastian, T. S., Gary, D. E., White, S. M., & Hurford, G. J. 1998, Proc. SPIE, 3357, 609
- Belkora, L. 1997, ApJ, 481, 532
- Dulk, G. A., & Marsh, K. A. 1982, ApJ, 259, 350
- Eidman, V. Ya. 1958, Soviet Phys.-JETP, 7, 91
- . 1959, Soviet Phys.-JETP, 9, 947
- Fleishman, G. D., & Melnikov, V. F. 1998, Phys.-Uspekhi, 41, 1157
- . 2003, ApJ, 584, 1071
- Garibyan, G. M., & Goldman, I. I. 1954, Izv. Krymskoi Astrofiz. Obs., 7, 31
- Getmantsev, G. G. 1952, Dokl. Akad. Nauk. SSSR, 83, 557
- Ginzburg, V. L. 1953, Uspekhi Fiz. Nauk., 51, 343
- Ginzburg, V. L., & Syrovatsky, S. I. 1964, The Origin of Cosmic Rays (New York: Macmillan)
- Grebinskii, A. S., & Sedov, A. P. 1982, Soviet Astron., 26, 220
- Hewitt, R. G., Melrose, D. B., & Rönnmark, K. G. 1982, Australian J. Phys., 35, 447
- Hildebrandt, J., & Krüger, A. 1996, Kleinheubacher Berichte, 39, 717
- Kiepenheuer, K. O. 1950, Phys. Rev., 79, 738
- Klein, K.-L. 1987, A&A, 183, 341
- Korchak, A. A. 1957, Soviet Astron., 1, 360
- Korchak, A. A., & Syrovatsky, S. I. 1961, Astron. Zh., 38, 885
- Korchak, A. A., & Terletsky, Ya. P. 1952, Zh. Eks. Teor. Fiz., 22, 507
- Kundu, M. R., Nindos, A., White, S. M., & Grechnev, V. V. 2001, ApJ, 557, 880
- Lee, J., & Gary, D. E. 2000, ApJ, 543, 457
- Lee, J., Gary, D. E., & Shibasaki, K. 2000, ApJ, 531, 1109
- McTiernan, J. M., & Petrosian, V. 1991, ApJ, 379, 381
- Melnikov, V. F. 1994, Radiophys. Quantum Electron., 37, 557
- Melnikov, V. F., & Magun, A. 1998, Sol. Phys., 178, 153
- Melnikov, V. F., Reznikova, V. E., Yokoyama, T., & Shibasaki, K. 2002b, in Proc. SPM-10, Solar Variability: From Core to Outer Frontiers, ed. A. Wilson (ESA SP-506; Noordwijk: ESA), 339
- Melnikov, V. F., Shibasaki, K., Nakajima, H., Yokoyama, T., & Reznikova, V. E. 2001, in CESRA Workshop, Energy Conversion and Particle Acceleration in the Solar Corona, (Zurich: ETH), 17
- Melnikov, V. F., Shibasaki, K., & Reznikova, V. E. 2002a, ApJ, 580, L185
- Melnikov, V. F., & Silva, A. V. R. 2000, in ASP Conf. Ser. 206, High-Energy Solar Physics: Anticipating HESS1, ed. R. Ramaty & N. Mandzhavidze (San Francisco: ASP), 371, 475
- Miller, J. A., et al. 1997, J. Geophys. Res., 102, 14631
- Petrosian, V. 1981, ApJ, 251, 727
- Pryadko, J. M., & Petrosian, V. 1999, ApJ, 515, 873
- Ramaty, R. 1969, ApJ, 158, 753
- Ramaty, R., & Petrosian, V. 1972, ApJ, 178, 241
- Razin, V. A. 1960a, Izv. VUZov Radiofizika, 3, 584
- . 1960b, Izv. VUZov Radiofizika, 3, 921
- Robinson, P. A. 1985, ApJ, 298, 161
- Silva, A. V. R., & Valente, M. M. 2002, Sol. Phys., 206, 177
- Sokolov, A. A., & Ternov, I. M. 1956, Zh. Eksp. Teor. Fiz., 31, 473

- Syrovatsky, S. I. 1959, *Astron. Zh.*, 36, 17
Takakura, T. 1972, *Sol. Phys.*, 26, 151
Ter-Mikaelyan, M. L. 1954, *Dokl. Akad. Nauk. SSSR*, 94, 1033
Trubnikov, B. A. 1958, *Dokl. Akad. Nauk. SSSR*, 118, 913
Tsytovich, V. N. 1951, *Vestnik Mosk. Gos. Univ.*, 4, 27
Twiss, R. Q. 1954, *Philos. Mag.*, 45, 249
- Westfold, K. C. 1959, *ApJ*, 130, 241
Yokoyama, T., Nakajima, H., Shibasaki, K., Melnikov, V. F., & Stepanov, A. V. 2002, *ApJ*, 576, L87
Zhou, A.-H., Ma, C.-Y., Zhang, J., Wang, X.-D., & Zhang, H.-Q. 1998, *Sol. Phys.*, 177, 427
Zhou, A.-H., Huang, G.-L., & Wang, X.-D. 1999, *Sol. Phys.*, 189, 345